DOI: https://doi.org/10.37965/jdmd.2026.2245

A Study on Early Demagnetization Fault Diagnosis in Permanent Magnet Synchronous Motors Based on Two-Level Intelligent Optimization

Jintian Yin [1], Yiming Cao [1*], Li Liu [1*], Junfei Nie [1], JiongTang [1], Zhaoying Zeng [2]

1. Shaoyang University School of Electrical Engineering，Shao yang, Hunan，422000；

2. Hunan Baodong Agriculture and Animal Husbandry Technology Co., Ltd，Shao yang, Hunan，411000

*Corresponding author:caoyiming0322@163.com

Received 12 October , 2026; Revised 30 October ,2026; Accepted 19 November, 2026; Published online 24 November , 2026.

Abstract

Addressing the challenges associated with permanent magnet synchronous motors (PMSMs)—such as the faint characteristics of early demagnetization faults, which are difficult to detect against a background of strong noise, and the reliance of traditional diagnostic models on human experience and their limited capabilities—this paper proposes a new fault diagnosis method based on a two-layer intelligent optimization framework. In the first layer, the Gray Wolf Optimization (GWO) algorithm is introduced to adaptively optimize the number of modes K and the penalty factor α in Variational Mode Decomposition (VMD). With the objective of minimizing the local envelope entropy of the decomposition components, this approach enables the adaptive extraction of fault-sensitive features and effectively suppresses modal aliasing. On the second layer, the Moth-Fire Optimization (MFO) algorithm is used to automatically search for the optimal penalty parameter C and kernel parameter γ of the Support Vector Machine (SVM), with the goal of maximizing the average classification accuracy under 5-fold cross-validation, thereby constructing a high-precision fault classifier. Through Two-Tier Progressive Optimization Using GWO and MFO, we have established an end-to-end intelligent diagnostic chain spanning from signal decomposition to fault identification. Simulation and experimental results show that the proposed method achieves average diagnostic accuracy rates of 97.77% and 96.67%, respectively, on the test set, with an average diagnostic time of less than 0.65 seconds, significantly outperforming SVM models optimized using grid search and particle swarm optimization. This framework provides an effective solution for the intelligent and highly reliable early diagnosis of PMSM demagnetization faults.

Keywords: Permanent Magnet Synchronous Motor; Demagnetization Failure; Variational Modal Decomposition; Gray Wolf Optimization Algorithm; Moth-Flame Optimization Algorithm; Support Vector Machines; Troubleshooting

1. Introduction

Permanent magnet synchronous motors

DOI: https://doi.org/10.37965/jdmd.2026.2245

(PMSMs) are widely used in high-end manufacturing sectors such as new energy vehicles, aerospace, and industrial robotics due to their high efficiency, high power density, and excellent dynamic response characteristics [1]. However, as PMSMs operate for extended periods under complex conditions—such as high temperatures and heavy loads—the permanent magnets are susceptible to irreversible demagnetization, known as demagnetization failure, due to factors such as temperature, armature reaction, and mechanical vibration. Demagnetization not only leads to a decrease in motor output torque and reduced efficiency but, in severe cases, can even cause system failure, resulting in significant economic losses. Therefore, conducting research on the early diagnosis of PMSM demagnetization failures holds important engineering significance and academic value for ensuring the safe and stable operation of the system and reducing maintenance costs.

Currently, PMSM fault diagnosis methods are primarily divided into two categories: model-driven and data-driven. Model-driven methods rely on precise mathematical models; however, the highly nonlinear nature of motor systems and the coupling of multiple physical fields make precise modeling extremely difficult. In contrast, data-driven methods directly extract fault information from operational data, demonstrating greater adaptability and generalizability. Among these, stator current signals have become the preferred analysis target for fault diagnosis due to their ease of acquisition and rich information content. However, during the early stages of a fault, current features exhibit small amplitudes and low signal-to-noise ratios; therefore, effectively extracting weak fault features from a noisy background is a key challenge in achieving early diagnosis [2–5].

In the field of signal processing, Variational Mode Decomposition (VMD) has become a powerful tool for analyzing non-stationary signals due to its solid mathematical foundation and excellent noise-resistant performance. However, the effectiveness of VMD decomposition is highly dependent on the preset number of modes K and the penalty factor α; an inappropriate combination of parameters can lead to mode aliasing or information loss. To address this, intelligent optimization algorithms have been introduced to enable the automatic selection of VMD parameters. Among these, the Grey Wolf Optimizer (GWO) has demonstrated superior performance in parameter optimization problems due to its simple structure, fast convergence, and strong global search capability [6].

In the field of classification, Support Vector Machines (SVM) are widely used due to their outstanding performance in small-sample and nonlinear classification tasks [7]. However, the performance of SVMs is highly dependent on the selection of the penalty parameter C and the kernel parameter γ. Traditional grid search methods are inefficient, and the Particle Swarm Optimization (PSO) algorithm is prone to getting stuck in local optima. The Moth-Flame Optimization (MFO) algorithm is a novel swarm intelligence algorithm that features a small number of parameters and a balanced capability for both global search and local exploration, making it suitable for the efficient optimization of key SVM parameters [8-12]. The innovation of this paper lies in the development of a progressive, serial, two-layer optimization mechanism for the early diagnosis of mild demagnetization faults in permanent magnet synchronous motors.

Based on the above analysis, this paper proposes a two-layer intelligent optimization

DOI: https://doi.org/10.37965/jdmd.2026.2245

diagnostic framework that integrates GWO-VMD and MFO-SVM. The main contributions of this paper are as follows:

1.This paper proposes a GWO-VMD adaptive feature extraction method that utilizes the global optimization capabilities of GWO to automatically determine the optimal parameter combination for VMD, effectively separating the eigenmode functions sensitive to demagnetization faults from the raw current signal, and extracting energy entropy to construct fault feature vectors.

2. Develop an MFO-SVM intelligent classification model that uses the MFO algorithm to automatically search for the optimal hyperparameters of the SVM, thereby enhancing the classifier's ability to identify subtle fault features and improving its performance.

3. Through a two-layer progressive optimization mechanism that combines "adaptive decomposition" and "intelligent recognition," the system systematically addresses bottlenecks in traditional methods—such as strong parameter dependency, inadequate feature extraction, and poor model—to form an end-to-end intelligent diagnostic chain.

4. Through dual validation using both simulation and physical experimental platforms, the proposed method has been fully demonstrated to be superior in terms of diagnostic accuracy, computational efficiency, and engineering robustness.

2. Modeling of PMSM Demagnetization Faults and Simulation of Current Signals

2.1 Mathematical Model of a PMSM

Developing a mathematical model of a permanent magnet synchronous motor (PMSM) is the foundation for analyzing motor fault types. It aims to lay the theoretical groundwork for the development of a simulation platform for PMSM drive system fault models, thereby enabling the systematic collection of current data under fault conditions involving multiphysics coupling and providing high-confidence training samples for subsequent fault diagnosis algorithms [13].

To obtain high-quality current data covering various degrees of demagnetization, this paper establishes a mathematical model of a PMSM in the dq two-phase rotating coordinate system. The stator voltage equation and flux equation are as follows:

$$\begin{cases} u_d = R_s i_d + \dfrac{d\psi_d}{dt} - \omega\psi_q \\ u_q = R_s i_q + \dfrac{d\psi_q}{dt} + \omega\psi_d \\ \psi_d = L_d i_d + \psi_f \\ \psi_q = L_q i_q \end{cases} \tag{1}$$

Wherein, u_d and u_q are the d- and q-axis voltages, and i_d and i_q are the d- and q-axis currents; R denotes the stator resistance; L_d and L_q represent the d- and q-axis inductances (for surface-mounted PMSM, $L_d = L_q = L_s$); ω_e is the electrical angular velocity; ψ_f stands for the permanent-magnet flux linkage.

The electromagnetic torque equation and the rotor motion equation are, respectively:

$$T_e = \frac{3}{2} p_n \left[\psi_f i_q + (L_d - L_q) i_d i_q\right] \tag{2}$$

$$T_e - T_L = J\frac{d\omega_m}{dt} + B\omega_m \tag{3}$$

Wherein, p_n is the number of pole pairs; T_L denotes the load torque; J represents the moment of inertia; B stands for the damping coefficient [14].

DOI: https://doi.org/10.37965/jdmd.2026.2245

This paper uses a two-phase rotating coordinate system (dq) to build a simulation model in MATLAB/Simulink, as shown in Figures 1 and 2:

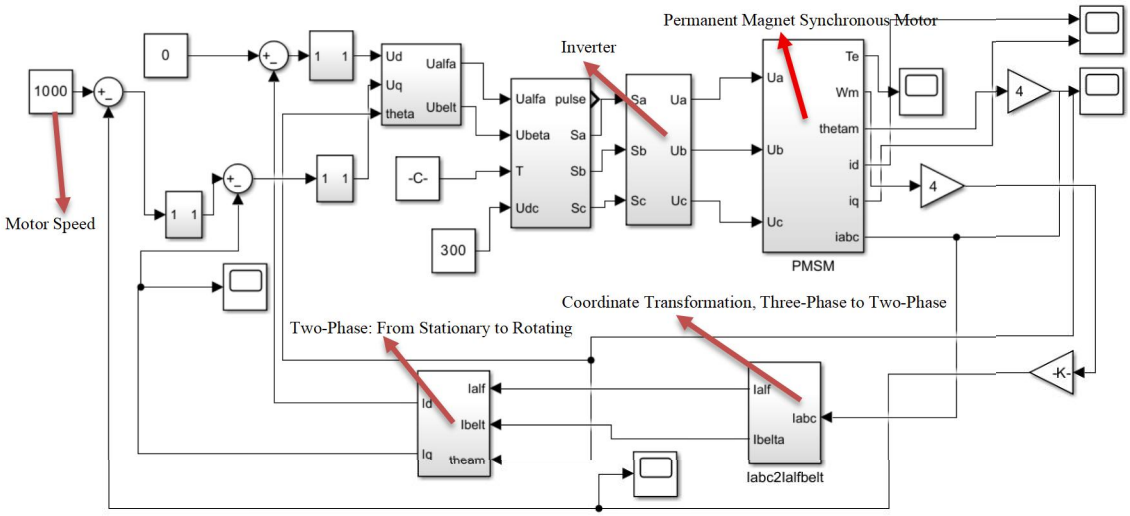


Figure 1: Standard Model of a Permanent Magnet Synchronous Motor

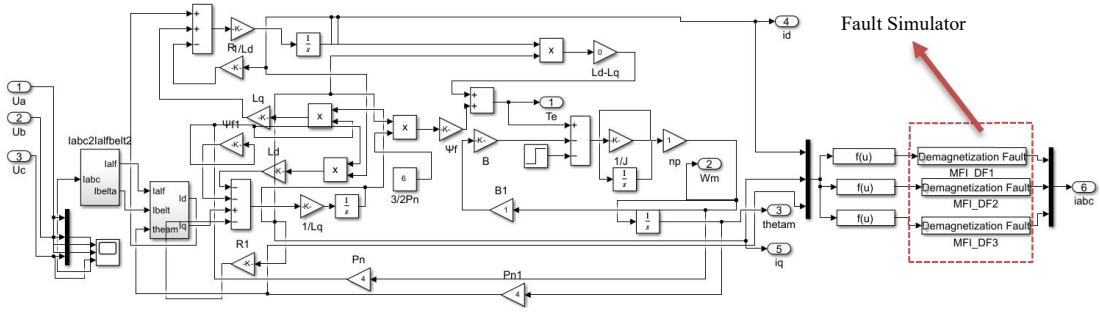


Figure 2: Model Incorporating a Demagnetization Fault Simulator

2.2 Equivalent Simulation of Demagnetization Faults

The demagnetization fault is directly manifested as the degradation of the permanent-magnet flux linkage ψ_f in the dq-axis coordinate system [15-17]. The demagnetization factor λ (0≤λ<1) is defined, and the equivalent flux linkage under the fault condition is given by:

$$\psi_f = (1-\lambda)\psi_{f0} \tag{4}$$

Wherein, λ=0 represents the healthy condition; λ=0.2 and λ=0.4 denote the light and

DOI: https://doi.org/10.37965/jdmd.2026.2245

moderate demagnetization faults with 20% and 40% flux-linkage degradation, respectively. Substituting Equation (4) into Equation (1), the variations in current response under different demagnetization severities can be simulated.

Parameter Name	Value
Polar Logarithm P_n	P_n=4
Stator Inductance	$L_d = L_q$ =0.0008 35
Stator Resistance R/Ω	R=2.875
Magnetic Flux /Wb	W_b =0.175
Moment of Inertia $J/kg\cdot m^2$	J=0.001
Damping Coefficient $b/(N\cdot m/rad/s)$	B=0.008

See Table 1 for the parameters of the permanent magnet synchronous motor:

Table 1: Parameters of Permanent Magnet Synchronous Motors

3 Adaptive Feature Extraction Based on GWO-VMD

3.1 Principles of Variational Mode Decomposition (VMD)

Due to the weak nature of early-stage fault current signals and their low signal-to-noise ratio, it is necessary to decompose and enhance their features. After comparing various algorithms, we propose an adaptive VMD parameter method based on the Gray Wolf Optimization (GWO) algorithm. VMD is mathematically rigorous and highly robust to noise; compared to Empirical Mode Decomposition (EMD), it can effectively suppress modal aliasing and endpoint effects, making it suitable for non-stationary current analysis. However, its performance depends on the number of modes k and the penalty factor α, and manual parameter setting can easily lead to information loss. Since GWO converges quickly, performs strong global searches, and is less prone to premature convergence—outperforming the Marine Predator Algorithm (MPA)—it is employed for the joint optimization of the two VMD parameters [18-20].

VMD iteratively solves a variational problem and decomposes the input signal $f(t)$ into K sparse intrinsic mode functions (IMFs) $u_k(t)$. Its constrained variational model is given by:

$$\min_{\{u_k\},\{\omega_k\}} \left\{ \sum_k \left\| \partial_t \left[\left(\delta(t) + \frac{j}{\pi t} \right) * u_k(t) \right] e^{-j\omega_k t} \right\|_2^2 \right\}, \text{s.t.} \sum_k u_k = f \tag{5}$$

Wherein, ω_k denotes the central frequency of the k-th IMF. By introducing the quadratic penalty factor α and Lagrange multiplier λ, the above-mentioned optimization problem is solved using the alternating direction method of multipliers (ADMM).

3.2 GWO Optimizes VMD Parameters

The decomposition performance of VMD is highly dependent on the parameters [K, α]. Too small parameter values will result in under-decomposition, while excessively large values will cause over-decomposition [21]. To address this issue, the Grey Wolf Optimizer (GWO) algorithm is introduced for adaptive parameter optimization.

3.2.1 Grey Wolf Optimizer (GWO)

GWO simulates the social hierarchy and hunting behavior of grey wolf packs. Within the solution space, the optimal, sub-optimal, and third-best solutions are defined as the α, β, and δ wolves, respectively, while the remaining candidate solutions correspond to the ω wolves. The position-update formula is given by:

DOI: https://doi.org/10.37965/jdmd.2026.2245

$$\vec{D} = \left| \vec{C} \cdot \vec{X}_p(t) - \vec{X}(t) \right|,$$
$$\vec{X}(t+1) = \vec{X}_p(t) - \vec{A} \cdot \vec{D}$$

Wherein, $\vec{X}_p$ denotes the position of the prey; $\vec{A}$ and $\vec{C}$ are coefficient vectors.

3.2.2 Fitness Function Design

Local envelope entropy is a practical optimization objective used to guide VMD in separating fault-sensitive harmonic bands from background noise and irrelevant components, rather than relying on the pulse sparsity of the fault itself [22]. For the k-th decomposed IMF component $u_k(t)$, its envelope entropy E_p is defined as:

$$E_p = -\sum_{n=1}^{N} p_k(n) \log\left(p_k(n)\right),$$
$$p_k(n) = \frac{a_k(n)}{\sum_{n=1}^{N} a_k(n)}$$

Wherein, $a_k(n)$ denotes the envelope signal obtained via the Hilbert transform of $u_k(t)$. The optimization objective of GWO is to minimize the minimum envelope-entropy value min (E_p) among all IMFs. This drives the algorithm to search for the [K, α] combination that yields the clearest IMF components. The optimization results are K=6 and α=1600.

3.3 Fault Feature Extraction

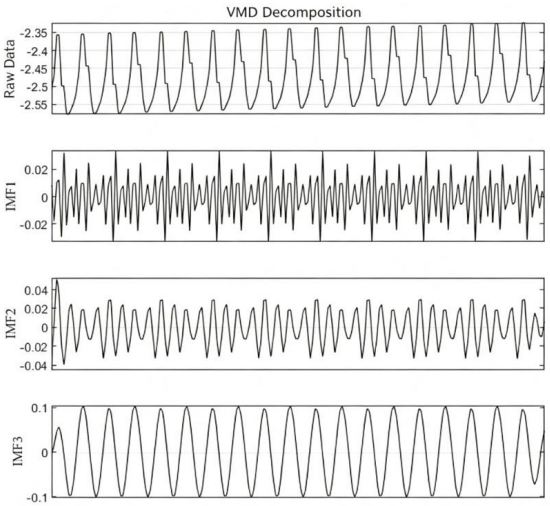
GWO-VMD is employed to decompose the three-phase current signals, yielding a set of IMFs. The energy of each IMF is calculated as $E_k = \sum \left| u_k(t) \right|^2$. After normalization, the energy entropy H is obtained and taken as the fault feature vector:

$$H = -\sum_{k=1}^{K} p_k \log(p_k), \quad p_k = \frac{E_k}{\sum E_k} \tag{8}$$

This eigenvector effectively characterizes the differences in the distribution of signal energy across various frequency bands at different levels of demagnetization.

As shown in Figure 3, it can be seen that when a minor fault occurs, the current waveform is highly similar to the normal waveform and is difficult to distinguish with the naked eye. Relying solely on traditional time-domain waveform comparison analysis is no longer sufficient to effectively identify faults. However, the GWO-optimized VMD algorithm can effectively decompose the raw waveform:

Figure 3: VMD-Decomposed Waveform



After decomposing the signal into six IMFs using GWO-VMD, we calculated the Pearson correlation coefficients between each IMF and the original current signal. IMFs with correlation coefficients below the threshold of 0.2 were considered noise-dominated components and were discarded, and the three IMFs with the highest correlations were retained for feature extraction.

As shown in Figure 4, a comparison of the convergence trends in iterative fitness between the two algorithms reveals that the GWO

DOI: https://doi.org/10.37965/jdmd.2026.2245

algorithm possesses stronger global optimization and in-depth local search capabilities. Its solution accuracy and convergence reliability are significantly superior to those of the MPA algorithm, making it more suitable for the adaptive optimization of key parameters in the VMD algorithm. It can effectively improve the quality of modal decomposition of motor fault signals under complex operating conditions, thereby providing higher-quality feature data support for subsequent high-precision fault diagnosis.

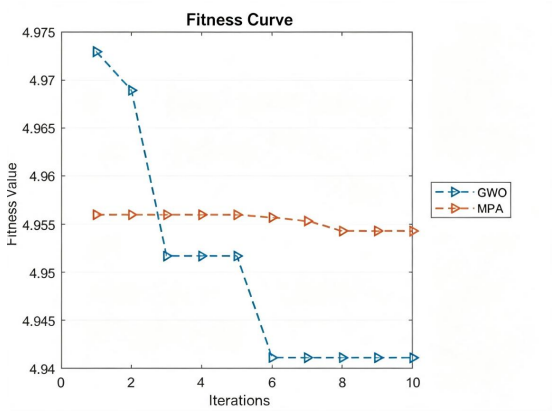


Figure 4: Fitness Curve

Compared to the Marine Predator Algorithm (MPA), GWO offers the following three advantages in VMD parameter optimization: (1) Faster convergence, with the algorithm continuously approaching the global optimum during the middle and late stages of iteration; (2) Fewer parameters requiring tuning (only population size and maximum number of iterations), making it easier to deploy in engineering applications; (3) When addressing multimodal non-convex optimization problems, its hierarchical guidance mechanism effectively balances global search and local exploration, reducing the risk of getting stuck at a local optimum. Therefore, this paper selects GWO for the joint optimization of VMD parameters.

4 An MFO-SVM-Based Fault Diagnosis Model

4.1 Basic Principles of Support Vector Machines (SVM)

The core idea of SVM is to find an optimal hyperplane that maximizes the margin between two classes of samples. For nonlinear problems, kernel functions are utilized to map data into a high- dimensional feature space. In this paper, the radial basis function (RBF) kernel $K(x_i, x_j) = \exp\left(-\gamma \| x_i - x_j \|^2\right)$ is adopted. Its optimization objective is given by:

$$\begin{cases} \min\limits_{\omega,b,\xi} \dfrac{1}{2} \| \omega \|^2 + C \sum\limits_{i=1}^{N} \xi_i \\ y_i \left(\omega^T \phi(x_i) + b \right) \geq 1 - \xi_i, \quad \xi_i \geq 0 \end{cases} \tag{9}$$

Wherein, $\frac{1}{2} \| \omega \|^2$ denotes the structural risk term for maximizing the classification margin; $\sum_{i=1}^{n} \xi_i$ represents the empirical risk term for minimizing the training error. The selection of the penalty parameter C and kernel parameter γ is the key to SVM performance [23-25].

4.2 MFO Optimization of SVM Parameters

4.2.1 Moth-Flame Optimization Algorithm (MFO)

MFO simulates the navigation mechanism of moths flying in a spiral around a flame (the optimal solution). The position update for each moth depends on its corresponding flame, and the formula for the spiral update is:

$$M_i = D_i \cdot e^{bt} \cdot \cos(2\pi t) + F_j \tag{10}$$

Wherein, M_i denotes the position of the i-th moth; F_j denotes the position of the j-th flame; $D_i = | F_j - M_i |$ represents the distance between them; b is the spiral shape constant; t is a random

DOI: https://doi.org/10.37965/jdmd.2026.2245

number in the range of [−1,1].

4.2.2Definition of feature vector fed into SVM

After GWO-VMD decomposition, we obtain K=6 intrinsic mode function components $\{u_1(t), u_2(t), \ldots, u_6(t)\}$ .Compute the energy of each IMF component:

$$E_k = \sum_t \left\| u_k(t) \right\|^2 \quad (1$$

Normalize the energy per unit mass, the energy entropy of each IMF is defined as:

$$H_k = -\tilde{E}_k \cdot \log_2(\tilde{E}_k) \quad (1$$

We screen valid IMF components from the 6 decomposed modes, and retain 3 effective IMFs. For the three selected IMFs, their normalized energy values $\tilde{E}_1, \tilde{E}_2, \tilde{E}_3$ and corresponding energy entropy values $H_1, \mathrm{H}_2, \mathrm{H}_3$ constitute the final feature vector. The actual input feature vector for SVM is $x = \left[\tilde{E}_1, \tilde{E}_2, \tilde{E}_3, H_1, H_2, H_3 \right]^T$ This 6-dimensional vector is further processed by Min-Max normalization and fed into the MFO-SVM classifier.

4.2.3MFO-Optimized SVM Fault Diagnosis Proces s

The workflow of the MFO-SVM fault diagnosis model developed in this paper is as follows:

1.Feature Extraction: Based on the method described in Chapter 2, VMD decomposition is performed on the current signals of a PMSM under normal operating conditions and under fault conditions with varying degrees of demagnetization to extract energy and entropy statistical features, thereby constructing fault feature vectors.

2.Data Split: The feature samples were split into a training set and a test set in an 8:2 ratio and normalized to eliminate the effects of unit scale. This paper employs the Min-Max normalization method, which linearly maps the feature values to the interval [1, 3].

3.MFO Parameter Initialization: The moth population size and maximum number of iterations (e.g., 50) are predefined. The variable dimension is set to 2, corresponding to parameters C and γ. Furthermore, the search ranges for C and γ are specified as C∈ [0.1,1000] and γ∈ [0.01,100].

4.Fitness Function Design: To guide the MFO algorithm in finding the optimal parameters, the average classification error rate (1 - accuracy) under 5-fold cross-validation on the training set is used as the fitness function. The MFO algorithm optimizes the SVM parameters with the goal of minimizing this fitness function.

5.MFO Iterative Optimization: In each generation, the moths update their positions based on the flame's location, calculate their fitness, and update the flame set until the termination condition is met.

6.SVM Model Training and Testing: Substitute the optimal parameters (C, γ) obtained through MFO optimization into the SVM, train the final classification model, and evaluate its diagnostic performance on the test set.

5 Simulation Experiments and Analysis of Results

5.1 Experimental Setup and Comparison Methods

The experiment was conducted using the MATLAB/Simulink simulation platform. The system sampling frequency was set to 10 kHz, the motor speed to 1,000 r/min, and the simulation duration to 2 seconds. At 0.2 seconds, the load was stepped from 0 Nm to 3 Nm. The signal-to-noise ratio is set to SNR = 15 dB This noise level is chosen to simulate inverter

DOI: https://doi.org/10.37965/jdmd.2026.2245

switching ripple and sensor noise in practical drives. Three operating conditions were defined: normal operation, mild demagnetization (20% magnetic flux decay), and moderate demagnetization (40% magnetic flux decay). For each operating condition, 50 data points were collected, resulting in a total of 150 sets of raw current data. The data was divided into a training set and a test set in an 7:3 ratio; that is, 35sets (105 in total) were selected from each operating condition for the training set, and the remaining 45 sets were used for the test set. The numbers 1, 2, and 3 were used to denote the three motor operating states: normal, 20% demagnetization, and 40% demagnetization, respectively.

To verify the effectiveness of the MFO-SVM model, the grid-search ranges for the comparative method GS-SVM are set as $C \in [0.1,1000]$ (logarithmic step: $\log_{10} C_{step} = 0.2$) and $\gamma \in [0.01,100]$ (logarithmic step: $\log_{10} \gamma_{step} = 0.2$). For PSO-SVM, the number of particles is set to 30, the inertia weight w=0.8, the acceleration coefficients c1=c2=1.5, and the maximum number of iterations is 50. All comparative models employ the identical feature set extracted by GWO-VMD to guarantee experimental fairness.

We ultimately succeeded in obtaining the stator current fluctuation curves during the simulation run. By running the simulation model, we obtained the waveform diagrams of the three-phase stator currents, as shown in Figures 5 and 6:

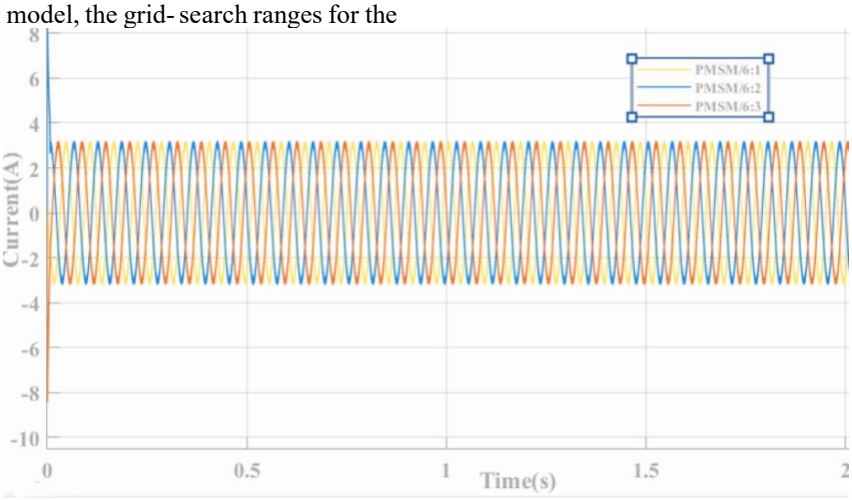


Figure 5: Normal Current Waveform

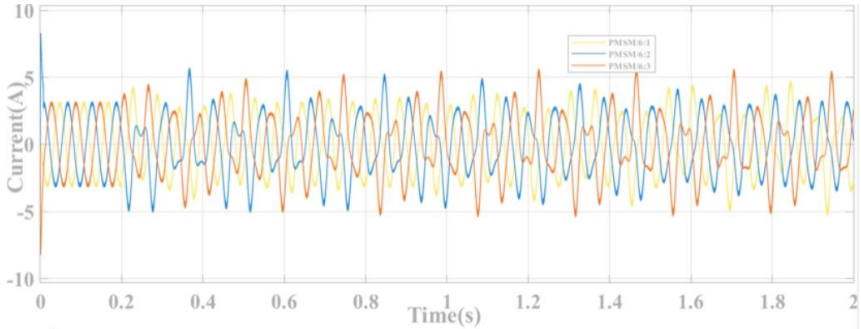


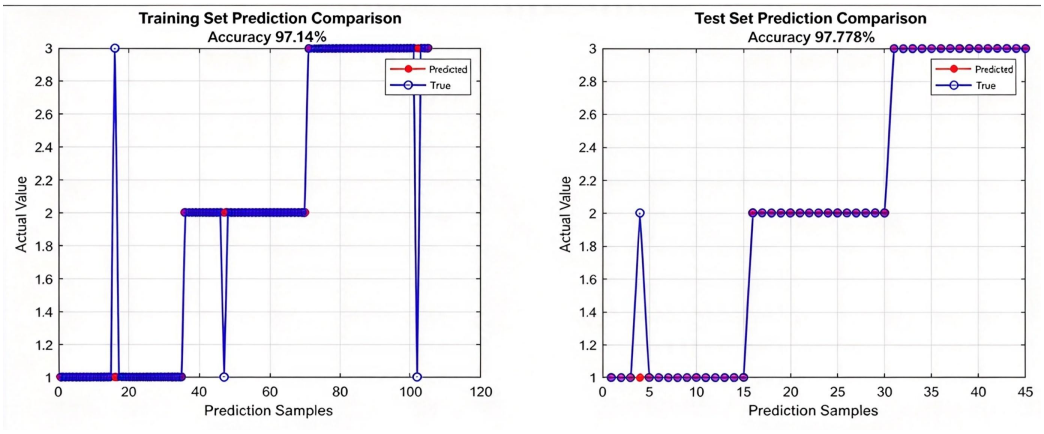
Figure 6: 40% Fault Current Waveform

5.2 Analysis and Discussion of Results

5.2.1 Diagnostic Accuracy and Efficiency

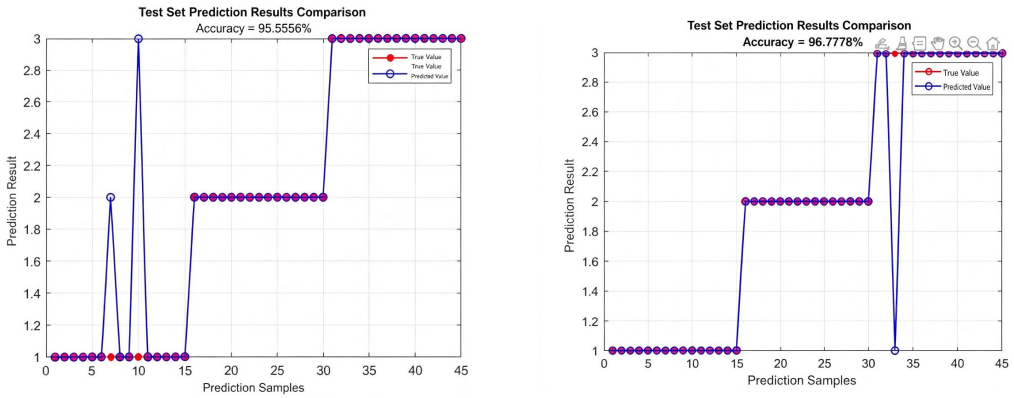
The experimental results for the different models are shown in Figures 7 and 8:

DOI: https://doi.org/10.37965/jdmd.2026.2245



(a) **(b)**

Figure 7: (a) MFO Optimizes SVM Training Results; (b) MFO-Optimized SVM Test Results



(a) **(b)**

Figure 8: (a) GS-Optimized SVM Test Results;(b) Test Results of PSO-Optimized SVM

The experimental results show that MFO-SVM outperforms both GS-SVM and PSO-SVM in terms of test accuracy and computational efficiency, with particularly outstanding performance on samples with mild demagnetization. This indicates that MFO can effectively identify optimal combinations of SVM parameters, thereby enhancing the model's ability to detect faint faults. The reported average diagnostic time in Table 2 corresponds to online inference time only: including GWO-VMD signal decomposition, IMF screening, feature-vector computation and SVM prediction, excluding the offline optimizer training / hyper-parameter searching procedure. Five independent repeated runs are executed, and the final value is the mean inference time over all test samples. (All competing models share the same GWO-VMD-extracted feature set. Hence this comparison mainly evaluates the performance of different SVM hyper-parameter optimization algorithms):

DOI: https://doi.org/10.37965/jdmd.2026.2245

Table 2: Comparison of the Performance of Different Diagnostic Models

Model	Optima C	Optima γ	Test Accuracy	Average Diagnosis Time (s)
GS-SVM	100	0.5	95.56%	1.72
PSO-SVM	85.3	0.42	96.78%	0.63
MFO-SVM	92.6	0.38	97.77%	0.54

5.2.2 Convergence and Robustness

The fitness curve for the MFO is shown in Figure 9. The algorithm converges rapidly within the first 10 iterations and remains stable in subsequent iterations, with the optimal fitness (cross-validation error rate) stabilizing at 0.062, demonstrating its high optimization efficiency and strong robustness.

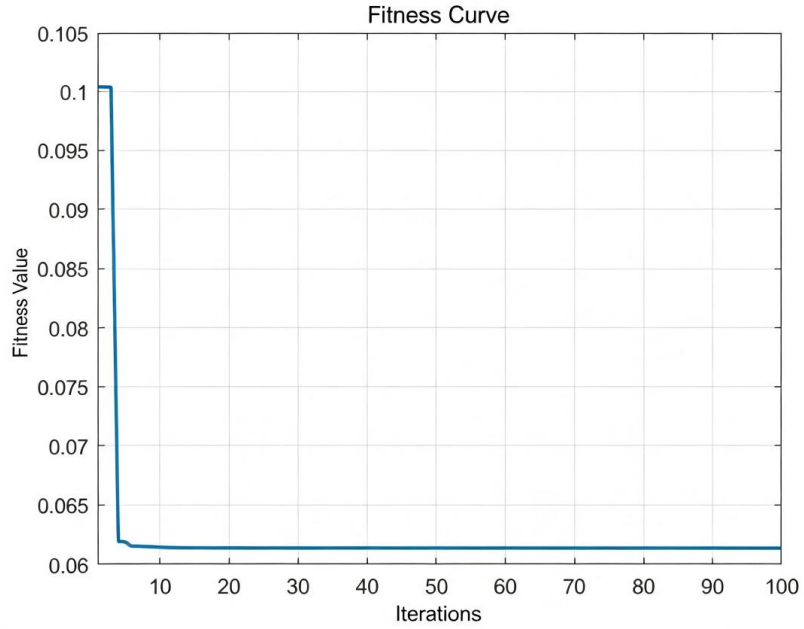
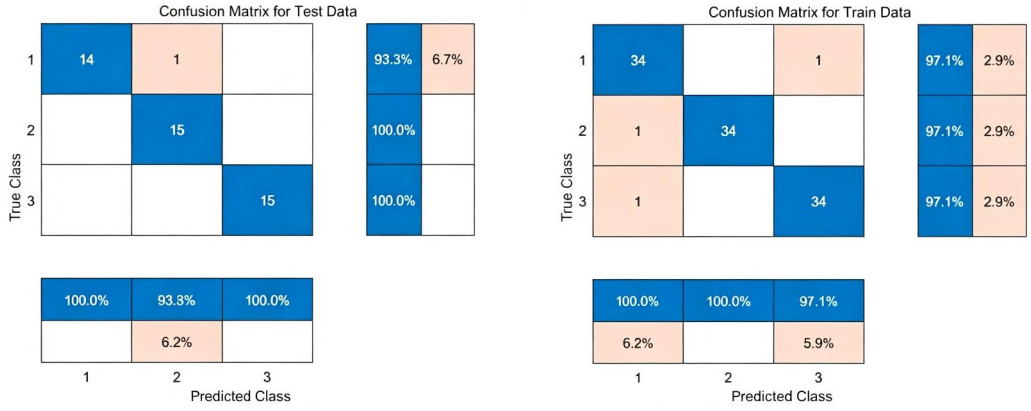


Figure 9: Fitness curve of the MFO-optimized SVM

5.2.3 Confusion Matrix Analysis

The confusion matrix for the MFO-SVM is shown in Figure 10. The recognition rates for all fault types exceed 95%; in particular, the recognition rate for mild demagnetization faults reaches 100%, demonstrating the model's excellent ability to distinguish faint faults.



DOI: https://doi.org/10.37965/jdmd.2026.2245

Figure 10: Confusion Matrix for MFO-SVM

6 Verification through hands-on experiments

6.1. Setting Up the Experimental Platform

To verify the effectiveness of the method in a real-world engineering environment, a motor testing platform was established. The platform consists of two PMSMs of the same model (one test motor and one load motor), a FMCON inverter, LEM current sensors, and an NI data acquisition card. The demagnetization fault was physically simulated using a high-temperature accelerated demagnetization method: the rotor was placed in a constant-temperature chamber and held at room temperature, 150°C, and 180°C for 72 hours each, resulting in three states: a normal motor, and motors with magnetic flux decay of approximately 20% and 40%. Flux loss is quantified via the no-load back-EMF test. The experimental sampling frequency and control conditions were consistent with those of the simulation. The motor test platform is shown in Figure 11:

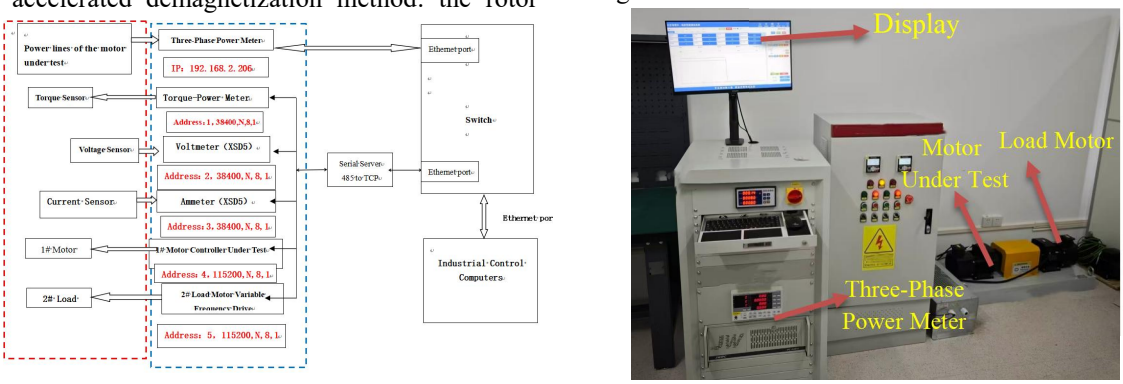


Figure 11: (a) System Wiring Diagram;(b) Motor Experiment Platform

6.2 Results of Physical Data Verification

When testing directly across datasets, the SVM decision function and normalization parameters obtained from simulation were completely discarded; we reconstructed the normalization method using statistical information from physical samples and trained the SVM from scratch based on physical features. The model parameters [C=92.6, γ=0.38] obtained from training on simulation data are directly adopted to test the real-world experimental data, yielding a classification accuracy of 95.33%. After the model is fine-tuned with the real-world training dataset, the parameters are updated to [C=88.1, γ=0.41], and the classification accuracy rises to 96.67%. Only one light demagnetization sample is misclassified. Detailed results are presented in Table 3.

Table 3: Comparison of Simulation and Physical Experiments

Data Source	Test Accuracy	Average Diagnosis Time (s)	Recall Rate for Mild Demagnetization	Moderate Demagnetization Recall Rate

DOI: https://doi.org/10.37965/jdmd.2026.2245

Simulation （MFO-SVM）	97.77%	0.54	100%	100%
Physical item （MFO-SVM）	96.67%	0.61	97.67%	100%

6.3 Discussion of Results

The accuracy of the physical experiments was slightly lower than that of the simulations, primarily due to:

1.Actual noise interference: Switching ripple from the variable-frequency drive (~8 kHz) and white noise from the sensor cause fluctuations in the signal envelope entropy.

2.Physical Deviations: There is a deviation of approximately ±2% between the actual demagnetization rate of permanent magnets and the nominal value, and there are manufacturing tolerances such as rotor eccentricity.

3. The diagnostic performance reported in this report applies only to conditions where the degree of demagnetization is at least 20% and the fixed-speed and load curves meet the definitions provided in this document, and not to arbitrary operating conditions. The generalizability of this method in complex scenarios, such as those involving variable speeds and variable loads, still requires further study.

Nevertheless, the proposed method maintained a high accuracy rate of 96.67% under real-world, non-ideal conditions, with a diagnostic time increase of only 0.07 seconds, fully demonstrating its excellent engineering robustness and potential for online monitoring. More importantly, the process from simulation to physical prototyping demonstrates that hyperparameters optimized through simulation can provide some reference value for physical modeling.

7 Conclusion

This paper addresses the challenge of diagnosing early-stage demagnetization faults in PMSMs by proposing a two-layer intelligent optimization diagnostic framework based on GWO-VMD and MFO-SVM. Through theoretical analysis and experimental validation, the following conclusions were reached:

1.The proposed GWO-VMD method can adaptively determine the optimal decomposition parameters for VMD, effectively extracting energy-entropy features sensitive to demagnetization faults, thereby addressing the bottlenecks of traditional methods, such as their strong parameter dependence and insufficient feature extraction.

2.The MFO-SVM model developed can automatically search for optimal hyperparameters, significantly improving the classifier's ability to detect minor faults, with a test set accuracy of 97.77%, outperforming traditional optimization methods.

3. The two-layer, progressive optimization mechanism we developed—"Adaptive Decomposition—Intelligent Recognition"—systemat sparsityically improves the performance of every stage in the diagnostic chain, Comparative results in Table 2 verify the superiority of MFO- SVM for classifier hyper- parameter searching under identical feature inputs. Further comparative analysis demonstrates the importance of adaptive parameter optimization for the VMD signal- decomposition layer.

4.lExperimental validation on a physical platform demonstrates that the proposed method exhibits good robustness against real-world noise

and physical deviations, achieving an accuracy rate of 96.67%. Furthermore, the fine-tuning process from the simulation model to the physical model is simple and effective, making it highly valuable for engineering applications.

Future work will focus on: 1) investigating the method's adaptability under more complex multi-fault coupling and varying operating conditions; 2) exploring model lightweighting techniques to enable deployment on embedded edge computing devices for real-time, online fault prediction.3) Conducting a comprehensive series of ablation experiments under standardized test conditions will further strengthen our conclusions, and this aspect of systematic ablation validation will be a priority in our future research.

Funding: Grant Projects：National Key Research and Development Program（2024YFB2505200）;Hunan Provincial Department of Education Project（24B0685）;Shaoyang City Science and Technology Program Projects(2024GZ2010,2025GZ3029);Corporate Collaborative Projects(2024HX295);

About the Author：Jin tian Yin, male, professor, Ph. D, Engaged in research on faults in traction drive control systems；E-mail: yinjintian0115@163.com

Yiming Cao, male, master's student, Engaged in research on faults in permanent magnet synchronous motors; E-mail: caoyiming0322@163.com

CONFLICTOFINTERESTSTATEMENT

The authors declare no conflicts of interest

References

[1] Ebrahim H E, Kour G, Khera P, et al. Fuzzy Logic Driven Self-Tuned PI Controller for Enhanced Speed Regulation of PMSM Drives[J]. Journal of Electrical and Computer Engineering,2026,2026(1):7690514-7690514.

[2] Haba T, Bertók Z, Budai C. A generalization of the Whittaker–Shannon interpolation formula for non-bandlimited signals[J]. Mechanical Systems and Signal Processing,2026,258114701-114701.

[3] Zhu Y, Liang H, Meng L. Temperature estimation and hot-spot forecasting of PMSM based on physics-informed neural network [J].

[4] Applied Thermal Engineering,2026,303(P4):132461-132461.

[5] Yang Z, Zhang X, Zhang Y. Demagnetization Fault Diagnosis Based on Coupled Multi-Physics Characteristics of Aviation Permanent Magnet Synchronous Motor[J]. Aerospace, 2025,13(1):39-39.

[6] Kolano J K, Drzymała B, Gęca J, et al. Current Sensor Fault Diagnosis in PMSM Drives Without Additional Hardware[J]. Energies, 2025,18(23):6298-6298.

[7] Kumar B N, Babu V R A, Kumar A B M, et al. Hybrid digital twin-based fault diagnosis framework for PMSMs in electric vehicle applications[J]. Franklin Open,2025,12100328-100328.

[8] Çelik B, Kara T. A review of fault-tolerant control methods for permanent magnet synchronous motors with demagnetization fault[J]. International Journal of Dynamics and Control,2025,13(7):277-277.

[9] Yu Y, Yuan C, Zeng D, et al. Conceptual Approach to Permanent Magnet Synchronous Motor Turn-to-Turn Short Circuit and Uniform Demagnetization Fault Diagnosis[J]. Actuators, 2024,13(12):511-511.

[10] Belgacem MA, HadefM, AliE, et al. Fault diagnosis of inter-turn short circuits in PMSM based on deep regulated neural network[J]. IET Electric Power Applications,2024,18(12):1991-2007.

[11] Zhang M, Cheng X, Xiao F, et al. Robust Detection for Demagnetization Fault in the Permanent-Magnet Synchronous Motor Using Improved Sliding-Mode Observer: Regular Papers[J].Journal of Advanced Computational Intelligence and Intelligent Informatics,2024,28(4):920-928.

[12] A. L H A, Abdulhady A J, N. M H, et al. Vibration-current data fusion and gradient bo

osting classifier for enhanced stator fault diagnosis in three-phase permanent magnet synchronous motors[J]. Electrical Engineering,2023,106(3):3253-3268.

[13] KERCHA S, AMEUR A, BENMILOUD I, et al. Detection of turn short circuit fault in PMSM variable speed sensorless vector control based on luenberger observer and adaptive Fuzzy Logic Controller[J]. Romanian Journal of Information Technology and Automatic Control,2023,33(4).

[14] Saha S, Kar U. Signal-Based Position Sensor Fault Diagnosis Applied to PMSM Drives for Fault-Tolerant Operation in Electric Vehicles[J]. World Electric Vehicle Journal,2023,14(5):123-.

[15] Belkhadir A, Pusca R, Belkhayat D, et al. Analytical Modeling, Analysis and Diagnosis of External Rotor PMSM with Stator Winding Unbalance Fault[J]. Energies, 2023, 16(7).

[16] Maciej S, Teresa O, T. C K. Diagnosis of Stator Winding and Permanent Magnet Faults of PMSM Drive Using Shallow Neural Networks[J]. Electronics, 2023,12(5):1068-1068.

[17] Ghosh S. Method for Fault Diagnosis and Speed Control of PMSM[J]. Computer Systems Science and Engineering,2022,45(3):2391-2404.

[18] Fule N, Yinquan Y. PMSM Demagnetization Fault Diagnosis Based on Back-EMF Signal[J]. Journal of Physics: Conference Series,2022,2395(1).

[19] Xudong Z, Xiaoming L, Xiaoqin Z. Current Sensor Fault Diagnosis and Tolerant Control for Nine-Phase PMSM Drives Based on Improved Axis Rotation[J]. Energies, 2022,15(13):4671-4671.

[20] Xinglong C, Peng Q, Yongyi C, et al. Inter-Turn Short Circuit Fault Diagnosis of PMSM[J]. Electronics, 2022,11(10):1576-1576.

[21] Yinquan Y, Haixi G, Qiping C, et al. Demagnetization Fault Detection and Location in PMSM Based on Correlation Coefficient of Branch Current Signals[J]. Energies, 2022,15(8):2952-2952.

[22] Zhiwen C, Ketian L, Tao P, et al. Multi-Condition PMSM Fault Diagnosis Based on Convolutional Neural Network Phase Tracker[J].Symmetry,2022,14(2):295-295.

[23] Fan X, Jing H, Miaoying Z. Demagnetization Fault Diagnosis of Permanent Magnet Synchronous Motor with Inductance Disturbance[J]. jaciii,2021,25(5):647-654.

[24] Kamila J, Mateusz D. A Current Sensor Fault Tolerant Control Strategy for PMSM Drive Systems Based on Cri Markers[J]. Energies, 2021,14(12):3443-3443.

[25] HaiXi G, YinQuan Y. Numerical study of electromagnetic force density of permanent magnet synchronous motor under demagnetization fault[C]//SPIE,2021.